

Oscillating spatial dependence of domain memory in ferromagnetic films mapped via x-ray speckle correlation

Karine Chesnel,¹ Joseph A. Nelson,¹ Stephen D. Kevan,² Matthew J. Carey,³ and Eric E. Fullerton⁴

¹*Department of Physics & Astronomy, Brigham Young University, Provo, Utah 84602, USA*

²*Department of Physics & Astronomy, University of Oregon, Eugene, Oregon 97403, USA*

³*Hitachi Global Storage Technologies, San Jose, California 95135, USA*

⁴*Center for Magnetic Recording Research, University of California, San Diego, La Jolla, CA 92093-0401, USA*

(Received 14 October 2010; revised manuscript received 25 November 2010; published 28 February 2011)

Magnetic domain memory (MDM) is observed in a Co/Pd ferromagnetic film when subject to exchange couplings with an IrMn antiferromagnetic layer. Our study uncovers the spatial and field dependence of the MDM at the nanoscopic scale. We found the degree of MDM to be extremely high (over 92%) at the scale of the domain periodicity, about 400 nm, and in the coercive region of the magnetization cycle, at about 1000 Oe. Furthermore, we observed an unusual spatial oscillation in the MDM, revealing a superstructure in the memory correlation at about 1.5 μm .

DOI: [10.1103/PhysRevB.83.054436](https://doi.org/10.1103/PhysRevB.83.054436)

PACS number(s): 75.70.-i, 75.50.Ss, 75.60.-d

Memory, the ability of a material to retrieve its configuration after cycling external parameters, generally results from complex internal dynamical processes.¹ Various systems—including shape-memory alloys, protein molecules, and magnetic materials—exhibit memory despite having a multitude of microscopic, interacting degrees of freedom.² The processes producing memory in soft, hard, and biological materials represent an intriguing aspect, motivating the implementation of experimental probes on varying length scales. We demonstrate here a unique tool to investigate magnetic domain memory (MDM)—the propensity of domains to retrieve their microscopic configuration after field cycling—in ferromagnetic films. Memory is here induced by exchange couplings and occurs in zero-field cooling. Our x-ray speckle correlation approach reveals an unusual oscillation in the MDM as a function of scattering wave vector, indicating a superstructure. The MDM is found to be very high over wide spatial and field ranges, and remains robust up to the blocking temperature.

Ferromagnetic (FM) films with perpendicular magnetization offer robust, technologically significant model systems³ to investigate memory phenomena, as they form nanoscale magnetic domain patterns⁴ that can be easily cycled with an external magnetic field (H). MDM was observed in Co/Pt multilayers and statistically quantified using soft-x-ray magnetic speckle metrology.⁵ Films exhibited partial return point memory (RPM),⁶ which revealed an intrinsic correlation between the structural defects and domain nucleation processes. Recently,⁷ we showed that MDM can be well controlled and fully optimized to a very high degree, over a wide range of field, by inducing exchange couplings⁸ with an antiferromagnetic (AF) sub-layer, which plays the role of a magnetic template.⁹

In these studies, memory was evaluated as a global statistical quantity, integrated over a broad range of length scales. The observed behavior of this global memory in exchange bias (EB) films as a function of applied field raises several questions: Does the FM layer retrieve the same magnetic configuration at all spatial scales? Is the memory

stronger at the characteristic domain size than at other scales? Does the memory behave differently with an applied field and with temperature at these different scales?

To address these questions, we have exploited the spatial information contained in x-ray scattering patterns, and quantified RPM as a function of scattering wave vector Q , corresponding to spatial scales ranging from the size of domain walls to well beyond the domain periodicity.¹⁰ We have measured the evolution of this Q -selective memory as a function of H and temperature T .

MDM is measured here in a [Co/Pt]IrMn multilayer with perpendicular anisotropy.¹¹ Films were grown at Hitachi Global Storage by sputtering onto low-stress silicon nitride membranes. Films were made of four repeats of FM [Co(4 Å)/Pd(7 Å)]₁₂ multilayers, each separated by 24 Å of AF IrMn layers. The film parameters (thicknesses, number of layers) have been optimized to obtain a blocking temperature $T_B \sim 300$ K. Our bulk vibrating sample magnetometry (VSM) and magnetic force microscopy (MFM) measurements were carried out at Brigham Young University.

Figure 1(a) shows the magnetization behavior of the film, above and well below its blocking temperature T_B , which characterizes EB interactions. In the latter, the film was first demagnetized at 400 K and then zero-field cooled (ZFC) down to 20 K. The ZFC loop exhibits no macroscopic bias; however, its shape significantly differs from the 400 K loop, and shows an inflection occurring just above the remanant coercive point $H_{RC} \sim 450$ Oe. H_{RC} corresponds to the field one should apply, so that when released to $H = 0$, the net magnetization returns to zero ($M = 0$), as illustrated in Fig. 1(b). This inflection likely results from the demagnetized FM domain structure imprinted into pinned interfacial spins in the antiferromagnetic layer during the ZFC process, leaving a microscopic template with a particular $M = 0$ configuration.⁷ In the ZFC state, the film tends to maintain $M \sim 0$ near H_{RC} , to minimize the interfacial EB interactions.

A microscopic view of the magnetic structure, obtained by magnetic force microscopy, in Fig. 1(c), shows a labyrinth of magnetic striped domains. This image gives a qualitative

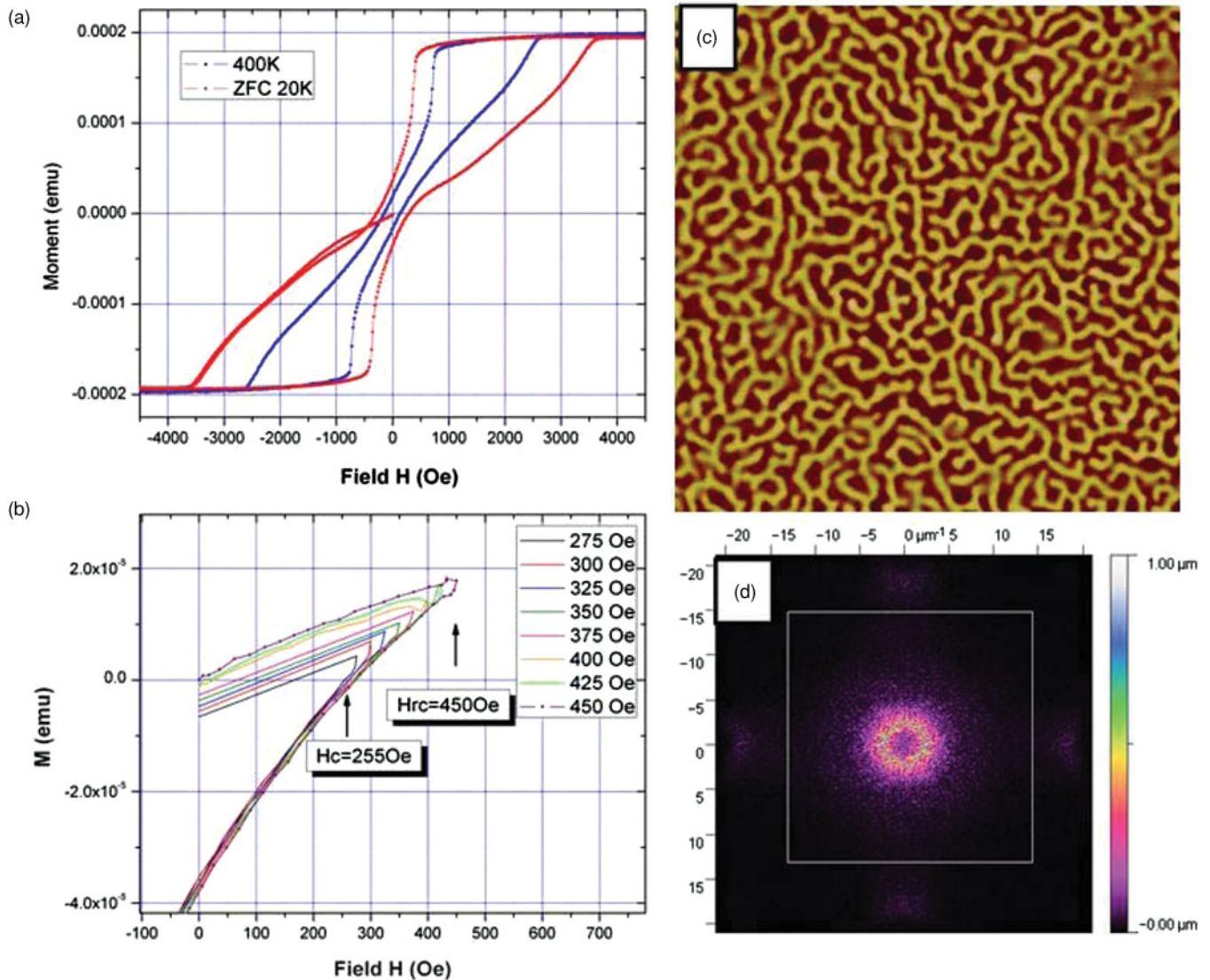


FIG. 1. (Color online) (a) Magnetization loop measured by VSM, at 400 K ($T > T_B$) and in ZFC state at 20 K after demagnetization at 400 K; (b) measurement of the remanent coercive H_{RC} point by gradual field increment; (c) $10 \times 10 \mu\text{m}^2$ MFM image measured at room temperature in the remanent state, showing the typical magnetic domain pattern which will later be imprinted; (d) Fourier transform of the MFM image shown in (c).

insight into the morphology of the magnetic pattern which will be imprinted in the AF layer during the ZFC. The Fourier transform in Fig. 1(d) confirms the isotropy of the domain pattern and indicates an average domain periodicity $p \sim 415$ nm. The ring's width determines the length over which the domains are correlated, here $l_c \sim 1.1 \mu\text{m}$.

The MDM was quantified using coherent soft-x-ray resonant magnetic scattering^{12,13} (C-XRMS). Figure 2(a) shows a scattering pattern measured in the ZFC state at $T = 20$ K and $H \sim H_{RC}$. The ring shape is related to the labyrinthine domain structure, similar to the Fourier transform in Fig. 1(d), except it offers better resolution and signal-to-noise ratio. The shape of the scattering pattern evolves from a disk, at nucleation, to a ring, from the coercive point until saturation. At $H \sim H_{RC}$, the ring reaches its maximum radius $Q = Q^* \sim 2.5 \mu\text{m}^{-1}$, and domain periodicity is minimum $p = p^* \sim 406$ nm. The envelope of the scattering signal is perfectly

reproduced throughout field cycles. However, its specific texture, known as speckle, does not reproduce. Arising from coherent diffraction processes, speckle patterns provide a unique fingerprint of the specific microscopic domain morphology. To quantify the degree of MDM, we isolate the speckle from the envelope. Figure 2(b) shows the pure speckle pattern extracted from the scattering signal in Fig. 2(a), using an iterative smoothing process. We then probe the length-scale-dependent memory by cross-correlating selected rings of specific radius Q from the speckle patterns, as inset in Fig. 2(c). We have carefully adjusted the width of the rings to optimize signal-to-noise ratio and Q resolution.¹⁰

Our coherent soft-x-ray resonant magnetic scattering measurements were performed in transmission geometry using linearly polarized light at beamline 12.0.2.2 at the Advanced Light Source, LBNL.¹⁴ This source offers a transversely coherent soft-x-ray flux that is sufficient to produce rich

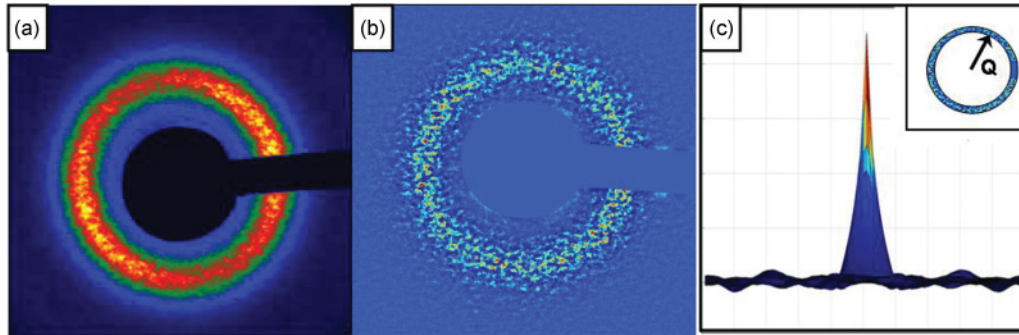


FIG. 2. (Color online) X-ray magnetic scattering and speckle correlation. (a) C-XRMS image, as collected on our CCD detector. This image is measured at the Co L_3 edge, with sample cooled in ZFC state at 20 K, and at H_{RC} . (b) Magnetic speckle fingerprint extracted from the scattering image (a) after removal of the incoherent scattering envelope. (c) Correlation pattern $\rho(\delta x, \delta y)$ resulting from cross-correlating isolated rings of same radius Q from two distinct speckle patterns (see inset).

speckle patterns that can be used to quantify the degree of reproducibility of magnetic domains. The photon energy was tuned to the Co L_3 edge (~ 780 eV) to optimize the magneto-optical contrast.¹³ The transmission scattering geometry probes the domain structure in the plane of the film with optimal sensitivity to the perpendicular component of magnetization.¹⁵ Furthermore, our C-XRMS setup includes an *in situ* magnetic field, so we can follow the evolution of the scattering signal along the full magnetization loop, with small field increments. Scattering patterns are collected on a CCD detector, located 0.95 m downstream of the sample.

Extending the cross-correlation approaches developed in optics,^{16,17} we quantify the Q -dependent RPM by cross-correlating isolated rings taken at the same Q , from two images A and B . The cross-correlation operation is defined as

$$A \otimes B = \sum_{x,y} A(x,y)B^*(-x + \delta x, -y + \delta y),$$

where A and B are the intensities of the respective images at pixel (x,y) , and $(\delta x, \delta y)$ is the displacement of one image with respect to the other. The output $A \otimes B$ is a two-dimensional pattern that can be mapped out as a function of $(\delta x, \delta y)$, as shown in Fig. 2(c). In practice, we perform this operation by using fast Fourier transforms. The correlation pattern exhibits a peak at the center, representing the amount of correlation between the two images. We then integrate the area under the peaks and form a normalized ratio using the autocorrelation signal of each image, thus defining the degree of correlation ρ :

$$\rho = \frac{\sum_{\delta x, \delta y} A \otimes B}{\sqrt{\sum_{\delta x, \delta y} A \otimes A \sum_{\delta x, \delta y} B \otimes B}}.$$

The amount of MDM is quantified by the normalized coefficient ρ , here estimated at given temperature T , field H , and ring size Q . Figure 3 shows the resulting $\rho(Q,H)$ maps at given T , where the color (gray) scale represents the amount of RPM. In Fig. 3(a), $\rho(Q,H)$ is measured along the ascending branch of the magnetization loop, so the domain reversal starts at low H (bottom of the map) and ends at high H (top of the map). The map shown in Fig. 3(a) was collected at 225 K.

Other correlation maps were collected at various temperatures from 30 K up to 335 K. A selection of these other maps is shown in Fig. 4.

To interpret a correlation map $\rho(Q,H)$, it is useful to compare it to its associate intensity map $I(Q,H)$, given in Fig. 3(b). $I(Q,H)$ represents the intensity of the speckles integrated over a given ring Q , at a given field value H , while $\rho(Q,H)$ quantifies how much the speckle distribution changes after field cycling, for the same Q and H . A first glance at the maps reveals that the behavior of $\rho(Q,H)$ differs significantly from the behavior of $I(Q,H)$. Indeed, the correlation $\rho(Q,H)$ does not mimic the intensity $I(Q,H)$, but exhibits different features with changing Q and H . This confirms that the amount of correlation ρ estimated from the speckle patterns is largely independent of the amount of intensity I present in the patterns at a specific point (Q,H) . Of course, the accuracy of the estimation of ρ depends somewhat on the amount of intensity I at a particular point—a better signal-to-noise ratio in the intensity will provide a better accuracy for ρ —and when the intensity is too low, it becomes impossible to estimate ρ , but for most of the (Q,H) space available on the maps, ρ is estimated with an accuracy higher than 97% (as explained further in the paper), and the field of view in (Q,H) is large enough to observe different behaviors for ρ and for I .

It is interesting to note that, while ρ and I exhibit different features on the maps, they share a similar trend along H . Going from nucleation to saturation along the vertical axis on the maps, both signals are generally low at the bottom, higher in the central region, and low at the top. Projecting the signal along the H axis leads to a low-high-low curve, as in Fig. 5(b), consistent with previous whole-image correlation results.^{7,18} This global behavior (integrated over Q) has been previously interpreted as evidence of the induction of MDM by exchange couplings.⁷ Now, by mapping $\rho(Q,H,T)$, we probe the MDM in further dimensions, revealing its dependence on spatial scales. The correlation technique used here quantifies the MDM as a function of Q —the wave vector in scattering space—and thus provides unique information, complementary to direct imaging techniques like x-ray microscopy,¹⁹ Kerr microscopy,²⁰ and photoelectron emission microscopy,²¹ where the structure and magnetic configuration of a film are generally sampled over smaller

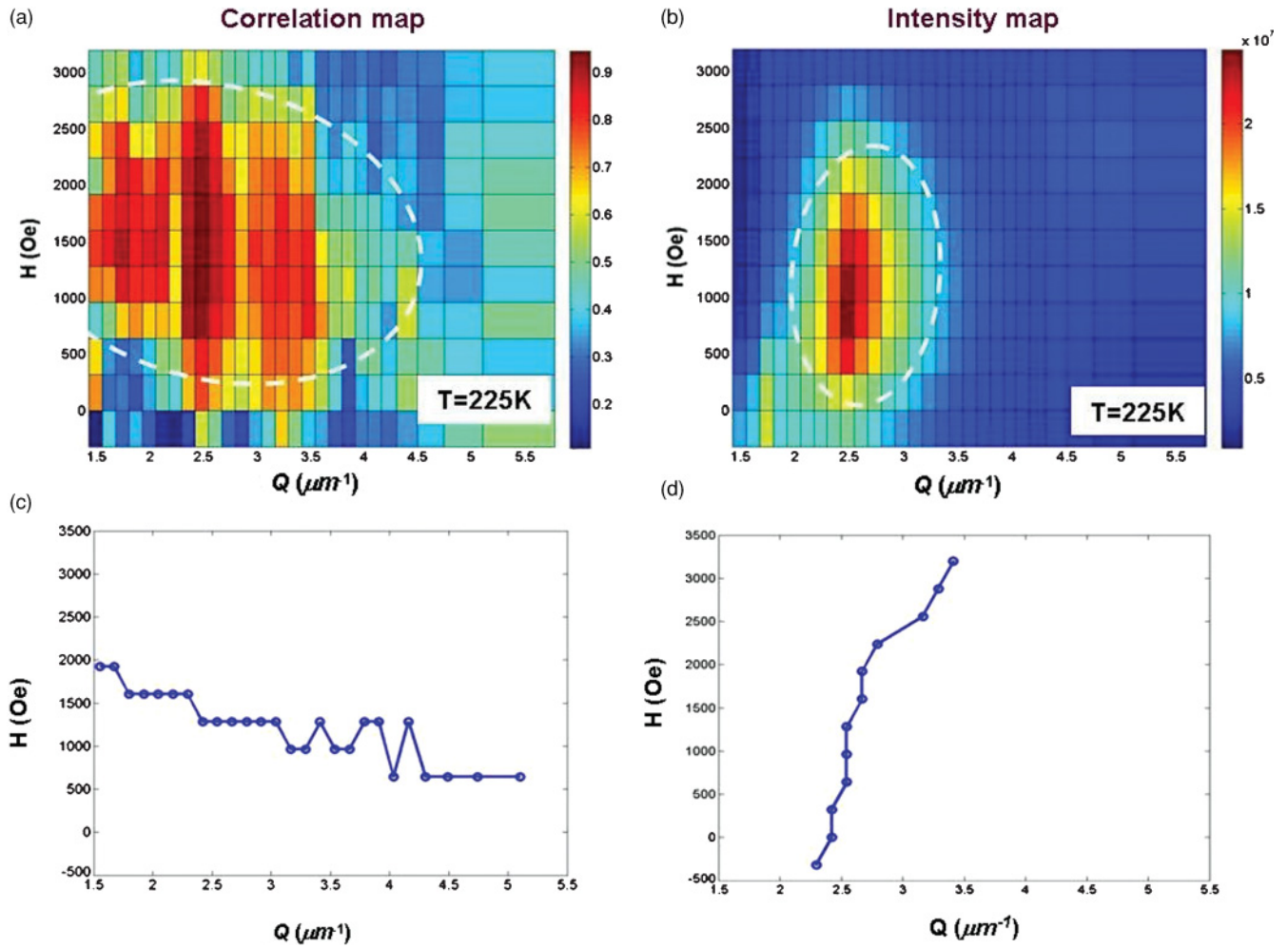


FIG. 3. (Color online) Correlation and scattering intensity maps. (a) Correlation map $\rho(Q,H)$ in ZFC state at 225 K; here RPM occurs along the ascending branch. (b) Corresponding intensity map $I(Q,H)$ at $T = 225$ K. (c) Directionality line connecting the peaks in fitted slices of the correlation map. (d) Directionality line connecting the peaks in fitted slices of the intensity map. In all maps, the vertical axis represents the magnetic field H and the horizontal axis represents the scattering vector Q (radius of the ring) at which the correlation is performed. As indicated by the sidebar, $\rho \sim 1$ (red - central region) means absolute memory, $\rho \sim 0$ (blue - outside region) means no memory.

local areas with less statistical information in terms of correlation lengths, or like MFM,²² providing only a superficial view of the magnetic configuration via magnetic stray fields.

Comparison of the correlation and intensity maps in Figs. 3(a) and 3(b) highlights several interesting results. First, $\rho(Q,H)$ is much more extended than $I(Q,H)$, as outlined by the dotted lines. On one hand, $I(Q,H)$ is concentrated in a relatively narrow peak located about $Q^* \sim 2.5 \mu\text{m}^{-1}$ and $H^* \sim 1000$ Oe. On the other hand, $\rho(Q,H)$ also peaks near (Q^*, H^*) , at over 92%, but extends over a much wider range of Q and H . Memory is strong not only at the periodicity p^* of the magnetic domains, but also at other spatial scales and for a wide range of field starting after nucleation and almost all the way to saturation.

A second compelling feature is the directionality of the signal: $\rho(Q,H)$ exhibits a trend downward to the right, as shown by the directionality line in Fig. 3(c) below the correlation map, while $I(Q,H)$ shows a trend upward to the right, as shown by the directionality curve in Fig. 3(d). These directionality curves have been calculated by locating the peak in the Gaussian fit

of successive slices from the respective maps. This striking difference in the directionality reveals that MDM occurs and progresses at different scales throughout the nucleation and reversal processes. At nucleation, $I(Q,H)$ is concentrated at low Q (disk pattern in the scattering image), and grows toward high Q values (ring pattern in the scattering image) when H increases toward saturation. The size of the low- Q disk patterns at nucleation corresponds to the average distance between nucleating domains, and could be modeled by a form function $S(q)$, typically used in diffuse scattering analysis. The radius of higher- Q ring patterns corresponds to the average period in the stripe domain patterns [as seen in Fig. 1(c)], obtained once the coercive point has been reached. Inversely, $\rho(Q,H)$ is located at higher Q values at nucleation, and progressively shifts toward lower Q when H increases. This spatial trend indicates that memory occurs first at short spatial scales, and extends to larger scales throughout the reversal process. At nucleation, domains form small bubbles located relatively far apart, and rather randomly, as suggested by the low ρ . However, there is higher correlation toward high Q , suggesting that even if

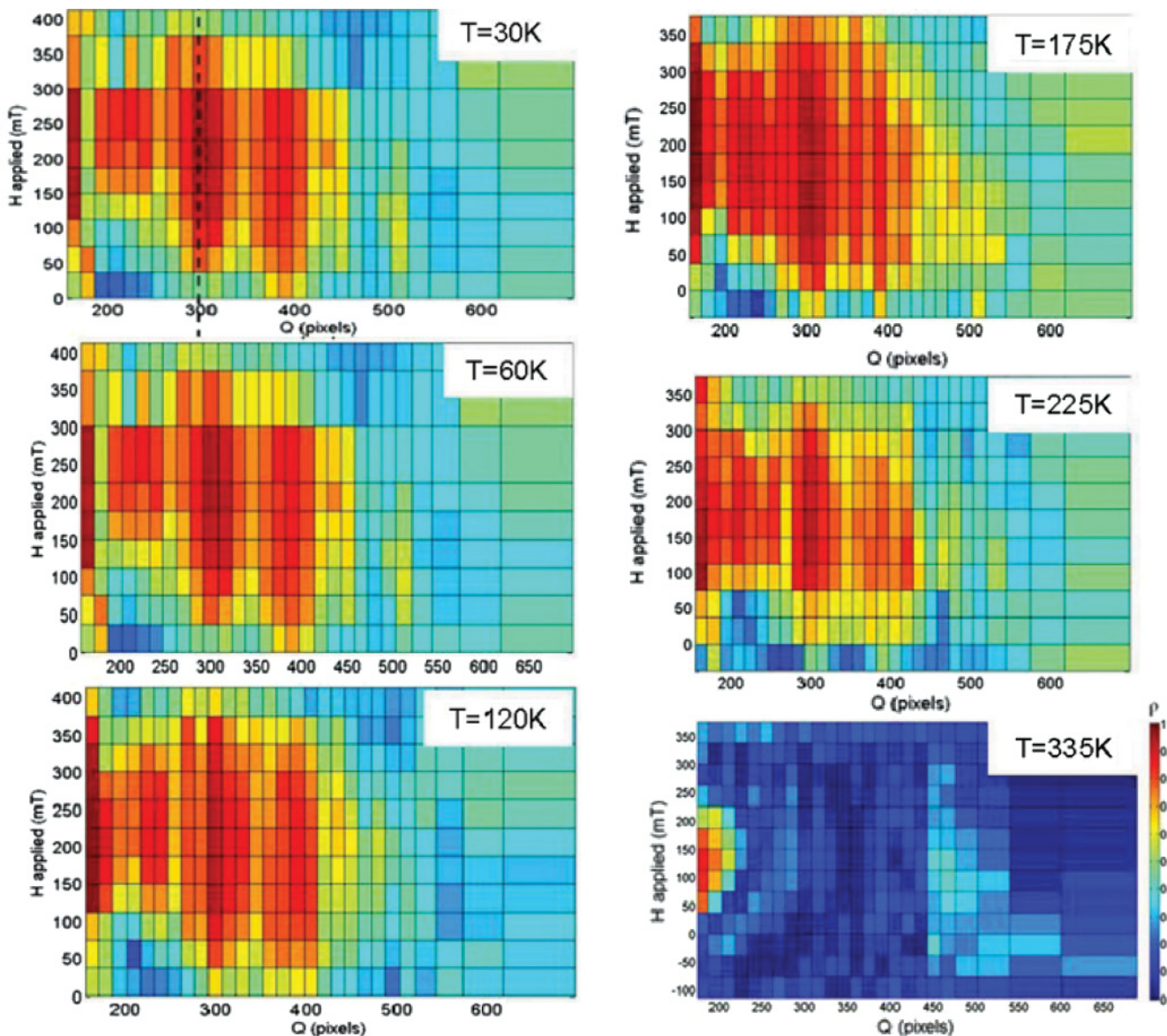


FIG. 4. (Color online) Correlation maps at different temperatures 30, 60, 120, 175, 225, and 335 K. All maps are measured along the ascending branch of the magnetization loop.

the bubbles nucleate at random locations, their individual shapes correlate at short scale, around 200 nm and smaller. When H increases through H^* , $\rho(Q, H)$ gets stronger around Q^* —the periodicity p^* of the magnetic domains is imprinted in the AF layer—and eventually in the lower- Q region, toward saturation. This suggests that memory expands from a short range (bubble phase) to the periodicity of the stripes, and toward longer ranges once the magnetic pattern is well fitted to the imprinted demagnetized pattern.

A third and most striking feature is the particular distribution of $\rho(Q, H)$, which does not decay smoothly like $I(Q, H)$, but exhibits multiple peaks. A cut at $H \sim H^*$ in Fig. 5(a) shows clearly several peaks, or an oscillation. The principal peak at Q^* is surrounded by two satellite peaks, separated by $q = 0.675 \mu\text{m}^{-1}$, which indicates a superstructure at $D = 1/q \sim 1.5 \mu\text{m}$, that is, about seven domains. This suggests that memory is periodically high at the length D . Interestingly,

this peak separation q almost matches the full width at half maximum of the peak in the scattering intensity, also plotted in Fig. 5(a). Thus, the MDM shows structure on a length scale that is comparable to the actual correlation length l_c of the domains topology. At higher Q values, for $Q \geq 2Q^*$, $\rho(Q)$ drastically decreases, indicating that, when $H \sim H^*$, the memory is low at short scales (< 200 nm). It suggests that domain walls in the FM layer only partially reproduce the topology of domain walls imprinted in the AF layer. However, the material exhibits almost perfect MDM at the scale of the stripe periodicity $p^* \sim 400$ nm and beyond, with an echoing effect on a length scale of $1.5 \mu\text{m}$.

A fourth attractive feature is the Q dependence of $\rho(H)$. Figure 5(b) shows vertical cuts at Q^* and $Q^* \pm q$. It indicates that long-scale memory ($Q < Q^*$) occurs more exclusively in the central field region (1000–2000 Oe) while the domain scale ($Q \sim Q^*$) and shorter-scale memory ($Q > Q^*$) extend over

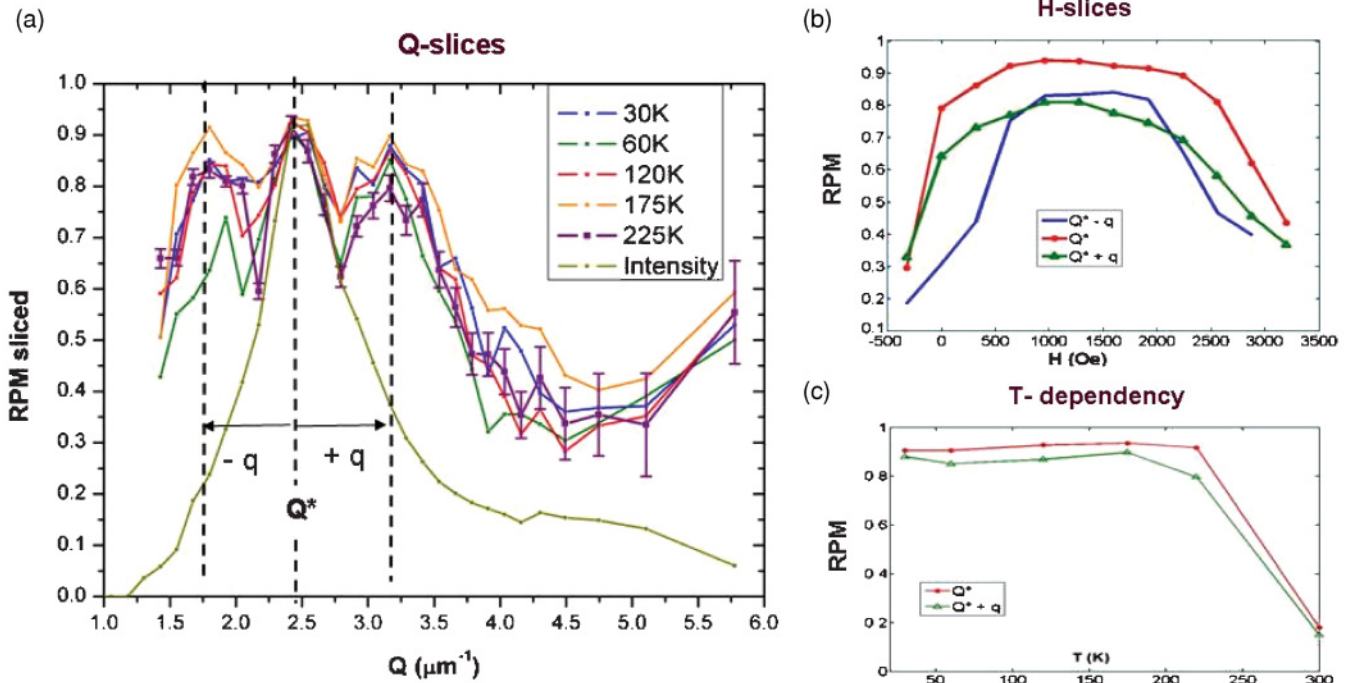


FIG. 5. (Color online) Q and H slices through maps and temperature dependency. (a) Q slices from the $\rho(Q,H)$ maps, in the coercive region ($H \sim H^*$), at different temperatures from 30 up to 225 K, and slice from the intensity $I(Q,H)$ at 225 K for comparison. Error bars are indicated on the 225 K slice. (b) H slices from the $\rho(Q,H)$ map at 225 K, at $Q = Q^*$ and $Q = Q^* \pm q$. (c) Maximum correlation value ρ with temperature T , for $Q = Q^*$ and $Q = Q^* + q$.

a wider field range. This magnetic morphology reproduces at short range, only once the system has passed through H_{RC} and is energetically stabilized.

To study potential thermal contributions to MDM, we have measured C-XRMS patterns at different temperatures from 30 up to 335 K. Figure 4 shows the correlation maps calculated for each temperature. We found that all $\rho(Q,H)$ maps at $T < T_B$ exhibit the same oscillation. The oscillation at 225 K in Fig. 3(c) shows more contrast than the oscillation at 30 K in Fig. 3(d), indicating a flatter spatial dependence at low T , and a possible thermal contribution enhancing the modulation at higher T . The cuts $\rho(Q)$ in Fig. 5(a) confirm that the oscillation is clearly visible at all temperatures, with an amplitude up to $\Delta\rho \sim 0.3$, demonstrating the reproducibility of the observed behavior and its steadiness through thermal variations when $T < T_B$. To verify that the observed oscillation is of physical nature, we have evaluated the error on the estimation of ρ . For this evaluation, we have considered two main contributions: first, the Poisson noise, associated with the signal-to-noise ratio in the intensity of the scattering signal for each selected ring; second, the error possibly introduced by the cross-correlation process on finite-size rings (“shot noise” at the central pixel of the correlation pattern). The resulting error is plotted together with the slice $\rho(Q)$ at 225 K. We find that the error stays very small in comparison to the amplitude of the oscillation. Indeed, the amplitude of the oscillation reaches up to $\Delta\rho \sim 0.32$ (or about 35% of ρ_{max}) at 225 K, while the estimated error in that region is only about 2%. The error stays within 3% for the main part of the Q range available and only increases up to 10% at high Q , when the scattering

intensity is very low. It is found that the Poisson contribution remains negligible (less than 0.07% of the error) for all Q and that the main contribution to the uncertainty on ρ comes from the correlation process, but stays within 3% in the region of interest and does not exceed 10% at very high Q . We therefore conclude that the observed oscillation is real. In addition, this oscillation appears at all temperatures below T_B . The maximum ρ value as function of T , plotted in Fig. 5(c) for the principal and right secondary peaks, indicates that the MDM stays constant and very high until the temperature approaches T_B . The measurement at 335 K, on the other hand, produces a very low degree of correlation ($\rho < 0.2$), demonstrating a thermally driven transition in the vicinity of T_B . For $T \geq T_B$, all exchange coupling effects vanish, resulting in the loss of memory. This confirms that the MDM is here mostly driven by exchange couplings below T_B and not by intrinsic structural defects in the film.

We suggest that the spatial dependence of the observed memory is influenced by the pattern imprinted in the AF layer during the ZFC. The characteristic size $D \sim 1.5 \mu\text{m}$ revealed by the MDM oscillation appears to match the distance over which the domains are morphologically correlated; however, this superstructural feature does *not* appear in the intensity maps. We infer that the distance D corresponds to an average distance between structural inhomogeneities, which translates into a specific correlation length imprinted in the AF domain pattern during the cooling. This length induces superstructural effects in the spatial dependence of RPM. These results demonstrate the possibility of inducing strong MDM at various spatial scales, from the characteristic size of magnetic domains to well

above it, and reinforcing it at specific scales by adjusting the magnetic morphology of reference template. While the average domain periodicity ($p \sim 400$ nm) is mainly dictated by the magnetic dipolar interactions in the ferromagnetic Co layers and the shape anisotropy, the characteristic oscillation length in the MDM ($D \sim 1.5 \mu\text{m}$) is an extra magnetic feature, most likely resulting from the exchange couplings between the FM and AF layers, combined with the structural inhomogeneities in the plane of the film at the micrometric scale. The observed MDM oscillation occurs in the range of $1 \mu\text{m}$, but it would be interesting to investigate next how nanometric variations in the thicknesses of the respective Co/Pd and IrMn layers, as well as their roughnesses, could possibly impact the size and the shape of the spatial features in the MDM.

In conclusion, our speckle correlation results bring unique insight into the spatial dependence of the MDM, unseen by bulk magnetization and microscopy measurements, nor by regular (incoherent) magnetic scattering. We find that MDM is globally strong over a wide spatial range centered about the magnetic stripe periodicity p^* , and over a large field range centered about H_{RC} . We also find that it is very robust at

all temperatures up to the blocking point T_B . Additionally, we find that it exhibits a surprising oscillation at micrometric scale, indicating that memory is strongly correlated to the magnetic domain periodicity but also to other characteristic lengths, dictated by the domain morphology of the underlying template.

These results suggest a variety of future investigations. One is to probe magnetic memory in field-cooled EB films and test if biasing effects alter the Q -dependent RPM. Also, one can study the dynamical behavior of the magnetic domain reversal near T_B , when the material is on the verge of losing its MDM, by measuring speckle temporal variations. Finally, one can investigate alternative approaches for creating nanostructured media to support the induction of magnetic memory. The broader impact of these studies lies in potential technological applications for magnetic data storage, but also in the advancement of the fundamental understanding of memory effects in condensed matter, both spatially and temporally.

E.E.F. was partially supported by DOE-BES Grant No. DE-SC0003678.

¹R. B. Laughlin, *A Different Universe: Reinventing Physics from the Bottom Down* (Basic Books, New York, 2005).

²R. B. Laughlin, David Pines, Joerg Schmalian, Branko P. Stojković, and Peter Wolynes, *Proc. Natl. Acad. Sci. U.S.A.* **97**, 32 (2000).

³H. Richter, *J. Magn. Magn. Mater.* **321**, 467 (2009).

⁴C. Kittel, *Phys. Rev.* **70**, 965 (1946).

⁵M. S. Pierce, C. R. Buechler, L. B. Sorensen, J. J. Turner, S. D. Kevan, E. A. Jagla, J. M. Deutsch, T. Mai, O. Narayan, J. E. Davies, K. Liu, J. Hunter Dunn, K. M. Chesnel, J. B. Kortright, O. Hellwig, and E. E. Fullerton, *Phys. Rev. Lett.* **94**, 017202 (2005).

⁶M. S. Pierce, C. R. Buechler, L. B. Sorensen, S. D. Kevan, E. A. Jagla, J. M. Deutsch, T. Mai, O. Narayan, J. E. Davies, Kai Liu, G. T. Zimanyi, H. G. Katzgraber, O. Hellwig, E. E. Fullerton, P. Fischer, and J. B. Kortright, *Phys. Rev. B* **75**, 144406 (2007).

⁷K. Chesnel, E. E. Fullerton, M. J. Carey, J. B. Kortright, and S. D. Kevan, *Phys. Rev. B* **78**, 132409 (2008).

⁸J. Nogués and I. K. Schuller, *J. Magn. Magn. Mater.* **192**, 203 (1999).

⁹P. Kappenberger, S. Martin, Y. Pellmont, H. J. Hug, J. B. Kortright, O. Hellwig, and E. E. Fullerton, *Phys. Rev. Lett.* **91**, 267202 (2003).

¹⁰J. Nelson, K. Chesnel, B. Wilcken, and S. Kevan (unpublished).

¹¹S. Maat, K. Takano, S. S. P. Parkin, and Eric E. Fullerton, *Phys. Rev. Lett.* **87**, 087202 (2001).

¹²F. de Bergevin and M. Brunel, *Acta. Crystallogr., Sect. A* **37**, 314 (1981).

¹³M. Blume, *J. Appl. Phys.* **57**, 3615 (1985).

¹⁴K. Chesnel, J. J. Turner, M. Pfeifer, and S. D. Kevan, *Appl. Phys. A* **92**, 431 (2008).

¹⁵J. B. Kortright, D. D. Awschalom, J. Stöhr, S. D. Bader, Y. U. Idzerda, S. S. P. Parkin, Ivan K. Schuller, and H. -C. Siegmann, *J. Magn. Magn. Mater.* **207**, 7 (1999).

¹⁶J. Goodman, *Statistical Optics* (Wiley, New York, 1985).

¹⁷K. S. Schmitz, *Introduction to Dynamic Light Scattering of Macromolecules* (Academic, San Diego, 1990).

¹⁸J. Nelson, B. Wilcken, and K. Chesnel, *J. Utah Acad. Sci., Arts Lett.* (2010).

¹⁹Mi-Young Im, Peter Fischer, Dong-Hyun Kim, Kyeong-Dong Lee, Sung-Hyun Lee, and Sung-Chul Shin, *Adv. Mater.* **20**, 1750 (2008).

²⁰Y. M. Chang, Minn-Tsong Lin, W. Pan, C. H. Ho, Y. D. Yao, O. de Haas, R. Schäfer, and C. M. Schneider, *J. Magn. Magn. Mater.* **239**, 375 (2002).

²¹J. Vogel, W. Kuch, M. Bonfim, J. Camarero, Y. Pennec, F. Offi, K. Fukumoto, J. Kirschner, A. Fontaine, and S. Pizzini, *Appl. Phys. Lett.* **82**, 2299 (2003).

²²L. K. Verma and V. Ng, *J. Magn. Magn. Mater.* **313**, 317 (2007).